Humic acid coated magnetic particles as highly efficient heterogeneous photo-Fenton materials for wastewater treatments

Nuno P.F. Gonçalves[a], Marco Minella[a,*], Debora Fabbri[a], Paola Calza[a], Cosimino Malitesta[b], Elisabetta Mazzotta[b], Alessandra Bianco Prevot[a,*]

[a] Dipartimento di Chimica, University of Turin, via P. Giuria 7, 10125, Torino, Italy
[b] Dipartimento di Scienze e Tecnologie Biologiche ed Ambientali, University of Salento, via Arnesano, I-73100, Lecce, Italy

HIGHLIGHTS

- The effect of HA coating on MPs was studied in (photo)-Fenton-like process.
- XPS allowed to relate iron surface speciation with (photo)-Fenton reactivity.
- Humic acid coating enhances the catalytic efficiency for 4-CP degradation.
- The efficiency of MP/HA was tested by degrading CECs in real wastewater sample.

GRAPHICAL ABSTRACT
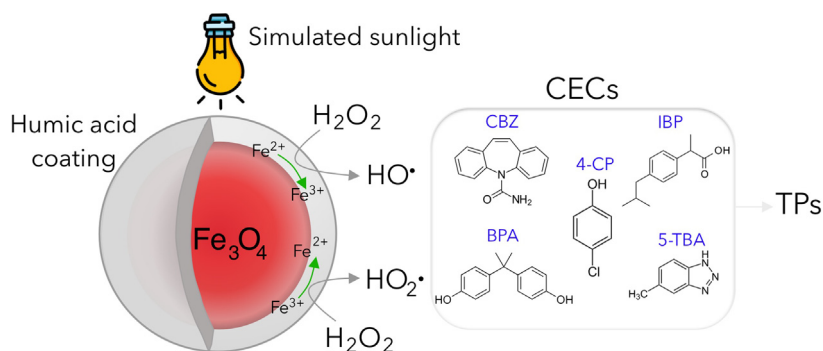
ABSTRACT

Heterogeneous photo-Fenton reaction with iron-based magnetic materials has been proposed as an alternative to the homogeneous Fenton process to remove contaminants of emerging concern (CECs) because of the low cost, facile recovery and reuse. The iron-based material is not only a reservoir to maintain an effective concentration of iron in solution, but it also activates H_2O_2 at the surface.

Magnetic particles (MPs) coated with different amount of humic acid (HA), prepared by co-precipitation method under anoxic and oxygenated conditions were synthesized. Their features were characterized by different techniques (XPS, XRD, TGA, SEM and FTIR). The ability of those materials to promote Fenton and photo-Fenton-like processes was investigated using 4-chlorophenol as standard substrate. The HA coating increased the catalyst efficiency, both in the dark and under irradiation, showing the best performance at pH below 4 under simulated sunlight. The iron speciation at the MPs surface had a paramount role in the H_2O_2 (photo)activation, although the processes promoted by the released iron in solution were not negligible on the overall degradation process. It was demonstrated a role of the surface defectivity to promote faster degradations as a consequence of not only a faster photodissolution, but also a higher heterogeneous reactivity promoted by defective sites.

The best performing MPs/HA showed high efficiency for the abatement of CECs, namely Carbamazepine, Ibuprofen, Bisphenol A and 5-Tolylbenzotriazole also in real wastewater. The obtained results demonstrated the potential application of the heterogeneous (photo)-Fenton process activated by these inexpensive and environmental friendly materials in advanced wastewater treatments.

* Corresponding authors.
  E-mail addresses: marco.minella@unito.it (M. Minella), alessandra.biancoprevot@unito.it (A. Bianco Prevot).

1. Introduction

Contaminants of emerging concern (CECs), including pharmaceuticals and personal care products, are increasingly being detected at low levels in surface water, groundwater and drinking water [1–3]. Despite their low concentration there is a real concern on the impact they may have on aquatic life and human health due to their toxicity [2,4]. As a consequence of their incomplete removal in the traditional wastewater treatment plants (WWTPs), considerable efforts have been devoted to develop purification methods capable of destroying these bio-recalcitrant contaminants.

Advanced oxidation processes (AOPs) have been attracting wide attention, since they are extremely efficient in the degradation/mineralization of organic contaminants, including several CECs, through the action of highly oxidizing species (mainly hydroxyl radicals, $\cdot$OH but also sulfate radical, $SO_4 \cdot^-$ or valence band holes in the case of heterogeneous photocatalysis) [5–9] able to react with CECs promoting their transformation into more biodegradable species easily removed in the conventional WWTPs.

Among AOPs there is increasing interest in Fenton, photo-Fenton and Fenton-like processes that generate highly reactive species [10–15] through the reactions between iron and H_2O_2 or other alternative oxidants (e.g. $S_2O_8^{2-}$) at acidic or even circumneutral pH, often in the presence of ligands able to form iron complexes [16–20]. The homogeneous Fenton reaction is interesting because Fe and H_2O_2 are environmentally friendly species, the reaction kinetic is usually fast and the process requires no complex reactors to be carried out. However, the reaction needs the pH adjustment to the optimum of 3 and subsequent neutralization with significant increment of the process cost [21]. Additionally, the formation of sludge to be removed and then dismissed increases the overall treatment cost and does not allow the recycling of the iron-based catalyst. H_2O_2 is activated by Fe^{2+} by electron transfer generating $\cdot$OH and Fe^{3+}. Even if the Fe^{2+} ions can be re-generated by H_2O_2 according to the reductive steps of the Haber and Weiss catalytic cycle [22], the reduction of Fe^{3+} to Fe^{2+} is usually the rate determining step of the process [18]. Consequently, the continuous addition of Fe^{2+} is necessary. Different strategies have been proposed to increase the rate of Fe^{3+} reduction. Among these, the ferric species can be photoreduced upon photolysis of dissolved Fe(III) [23] according to Eqs. (1–2).

$$Fe^{III} - L + h\nu \rightarrow Fe^{2+} + L^{\cdot+} \tag{1}$$

$$Fe(OH)^{2+} + h\nu \rightarrow Fe^{2+} + \cdot OH \tag{2}$$

Light induced Fe^{3+} reduction occurs with fast kinetics, thus overcoming the Fenton's limitation. Fe^{3+} can be indeed photo reduced to Fe^{2+} keeping the system catalytic.

Heterogeneous photo-Fenton reaction with iron-based magnetic materials and H_2O_2 has been proposed as a promising alternative to the homogeneous process [24]. The mechanism behind heterogeneous (photo-)Fenton reactions has not been fully assessed, and it is worth to be studied in deeper details. In particular, the role of the iron species in the operative catalytic cycle has been only partially clarified. The heterogeneous catalyst is often not only an iron reservoir able to maintain an effective concentration of iron in solution, but often its surface plays an active and catalytic role, as recently reported [10,25]. Furthermore, the chemical nature and the texture of the iron-based catalyst influence abruptly its activity affecting the working conditions (pH range, under irradiation *vs* dark activity, reusability…) [25,26]. Fe_3O_4 magnetic particles (MPs) used as iron-sources in Fenton and photo-Fenton processes have attracted significant interest due to their low cost, facile recovery (by means of a magnetic field) and reuse [12]. Recently, the potential application of MPs in heterogeneous Fenton and photo-Fenton processes for the removal of CECs has been investigated [25,27,28].

Magnetite is a mixed Fe(II)/Fe(III) oxide and it is well established that the Fe(II) ions in the structure are essential to activate heterogeneous Fenton-like processes [11,29]. The main problem using magnetite is the oxidation of Fe(II) to Fe(III) producing passive Fe(III) oxide layer inhibiting the catalytic activation of H_2O_2. In order to stabilize the Fe(II) surface species the use of organic coatings has been proposed [30]. Humic(-like) substances have been previously used to enhance the Fe_3O_4 stability, increase the dispersion and prevent the aggregation [31–33], even though the effective role played by humic (-like) substances in the oxidation mechanism is still not fully solved [7,34–38]. Recently, Aparicio et al. investigated the photo-Fenton oxidation of the psychiatric drug carbamazepine in the presence of core–shell magnetite-humic acids nanoparticles observing that the MPs were excellent iron sources to sustain the photo-Fenton process [39]. Moreover, Palma and co-workers investigated the H_2O_2 photo-activation on bio-based substances-magnetic iron oxide hybrid nanomaterials for the removal of caffeine concluding that the synthesized MPs allows the pollutant degradation at pH closer to neutrality, overcoming the limit of pH = 2.8 of the homogeneous photo-Fenton process [28].

In this study, humic acid (HA) coated Fe_3O_4 magnetic particles (Fe_3O_4/HA) were prepared through a co-precipitation method using different amounts of HA, both in anoxic and oxygenated conditions. The Fe_3O_4/HA materials were tested in aqueous media using 4-chlorophenol as a standard substrate, working at different pH, in the presence of H_2O_2, in the dark and under simulated solar irradiation. Additionally, the best performing material was tested for the removal of a CECs mixture both in artificial and real wastewater samples. For the first time a careful XPS analysis of the iron speciation of the MPs surface was carried out with the aim to correlate the diverse iron species at the surface with the reactivity of the synthesized materials to activate (in dark or under solar irradiation) H_2O_2.

2. Experimental

2.1. Materials

$FeCl_3 \cdot 6H_2O$ and $FeSO_4 \cdot 7H_2O$ were purchased from Carlo Erba Reagents; HA sodium salts (technical, 50–60%) from Aldrich-Chemie; 4-chlorophenol, Bisphenol A, Carbamazepine, Ibuprofen, 5-Tolylbenzotriazole, acetonitrile (gradient grade) and H_3PO_4 from Sigma-Aldrich. All the chemical reagents were used as received. Suspensions and standard solutions were prepared in Milli-Q® water.

The real wastewater samples were collected in a WWTP at the northern area of Italy (October 27th, 2017). The samples used were obtained from the outflow of the primary clarifier tank. This real sample was used after a rough pre-filtration step, carried out through a grade qualitative filter paper (Whatman) to remove large suspended solids and filtered using a hydrophilic 0.45 μm Sartolon Polyamide filter (Sartorius Biolab).

2.2. Materials synthesis and characterization

HA coated magnetite particles were prepared following the co-precipitation procedure reported in the literature with some minor modifications aiming to avoid the Fe^{2+} oxidation [31]. In detail, the MPs were prepared by co-precipitation method under nitrogen; 35 mL of a $FeCl_3 \cdot 6H_2O$ (6.42 g) and 4.17 g of $FeSO_4 \cdot 7H_2O$ water solution (molar ratio Fe(III)/Fe(II) = 1.5) were added to 65 mL of deoxygenated water at 90 °C, under vigorous mechanic stirring and N_2 continuous flow. Then, 10 mL of NH_4OH (25%) and 50 mL of HA solution at different concentrations were added rapidly and sequentially and a mixture of Fe(II) and Fe(III) hydroxides with adsorbed HA were co-precipitated. The mixture was kept for 30 min at 90 °C, and then cooled down to room temperature under continuous stirring and nitrogen flow. The obtained MPs were separated by centrifugation and washed with 40 mL of water five times. The MPs were dried in a Tube Furnace under nitrogen flow at 80 °C for 15 h to dry the materials and promote the formation of the oxidic lattice. The resulting MPs were manually

crumbled. Depending on the different wt.% of HA in the initial solution (namely 0.25 wt%, 0.5 wt%, 1 wt%, 2 wt% and 4 wt%), the obtained MPs were coded Fe_3O_4/0.25HA, Fe_3O_4/0.5HA, Fe_3O_4/1HA, Fe_3O_4/2HA, and Fe_3O_4/4HA, respectively. The bare Fe_3O_4 MPs were prepared with a similar procedure without the addition of HA solution. Materials coded ox-Fe_3O_4/0.5HA (addition of a 0.5 wt% HA solution) and ox-Fe_3O_4 (no addition of HA) were prepared with a similar procedure, but in air (both during the synthesis and drying process).

The morphology of the synthesized MPs was determined by scanning electron microscopy (SEM), with a Phenom Pro instrument operating at 5, 10 and 15 kV, 50.0 mA beam current and 50 pA probe intensity. Thermo-gravimetric analyses (TGA) were performed on a TA Q500 (TA Instruments), working under air atmosphere. The weight losses and the degradation profiles were evaluated by heating ca. 10–15 mg of each sample applying a heating ramp from 30 to 800 °C (rate 10 °C/min). X-ray diffraction (XRD) pattern of the powders were recorded with an Analytical X'PertPro equipped with an X'Celerator detector powder diffractometer using Cu K$_\alpha$ radiation generated at 45 kV and 40 mA. The 2θ range was from 20° to 100° (spinner mode) with a step size (2θ) of 0.03 and a counting time of 0.6 s. Fourier transform infrared (FTIR) were taken on a Bruker spectrometer recorded with 128 scans at 4 cm^{-1} for a wavenumber range of 4000 to 400 cm^{-1}. XPS measurements were recorded with an AXIS ULTRA DLD (Kratos Analytical) photoelectron spectrometer using a monochromatic AlKα source (1486.6 eV) operated at 150 W (10 kV, 15 mA). Base pressure in the analysis chamber was 5.3×10^{-9} torr. Survey scan spectra were recorded using a pass energy of 160 eV and a 1 eV step. High resolution spectra were acquired using a pass energy of 20 eV and a 0.1 eV step. The hybrid lens mode was used for all measurements. In each case the area of analysis was about $(700 \times 300) \mu m^2$. During the data acquisition a system of neutralization of the charge has been used. Processing of the spectra was accomplished by CasaXPS Release 2.3.16 software. For the analysis of high-resolution spectra all peaks were fitted using Shirley background and GL (30) lineshape (a combination of Gaussian 70% and Lorentzian 30%). For quantitative analysis, the relative sensitivity factors present in the library of CasaXPS for the areas of the signals were used. Surface charging was corrected considering adventitious C 1 s (binding energies (BE) = 285 eV).

2.3. Degradation procedure

The degradation experiments in Fenton-like condition were carried out in a beaker with a total volume of 50 mL protected from light under magnetic stirring, while experiments in photo-Fenton-like condition were performed in closed Pyrex glass cells filled with 5 mL under magnetic stirring and irradiated for different times (1 to 60 min) in a sunlight simulator (Solarbox, CO.FO.Me.Gra, Milan) equipped with a xenon lamp (1500 W) with a cut-off filter at below 340 nm. On top of the suspensions the irradiance was 18 W m^{-2} in the 295–400 nm range (similar to the natural sunlight UV irradiance at middle European latitude in sunny days) [40]. The suspension temperature was ~45 °C. Hydrogen peroxide (1.0 mmol L^{-1}) was added to the suspension of MPs (100 mg L^{-1}). The initial concentration of 4-chlorophenol (4-CP, pK$_a$ = 9.4 [41]) was 0.2 mmol L^{-1}. The pH was adjusted with H$_2$SO$_4$. After the reaction time, 0.33 mL of methanol were added to the 5 mL of the suspension to quench the thermal Fenton reaction, then the samples were filtered using a 0.45 μm filter (Sartorius, hydrophilic PTFE). An equilibration time of 30 min was always adopted to highlight possible adsorption and in dark degradation.

Degradation experiments with CECs were performed with initial concentration of 0.2 mmol L^{-1} for Ibuprofen (IBP, pK$_a$ = 5.3 [42]), Bisphenol A (BPA, pK$_a$ = 9.6 [43]), 5-tolylbenzotriazole (5-TBA, pK$_a$ = 8.6 for the conjugated acid [44]) and 0.1 mmol L^{-1} for Carbamazepine (CBZ, pK$_a$ = 13.9 [45]). Moreover, a degradation experiment in the same real matrix but on a mixture of these compounds was carried out with each CEC at an initial concentration 20 μmol L^{-1}. The

real waste water sample had total organic carbon (TOC) = 9.7 mg^C L^{-1}, Inorganic Carbon (IC) = 68.4 mg^C L^{-1}, Total Nitrogen (TN) 31.3 mg^N L^{-1} and pH = 8.3.

The degradation experiments were carried out in triplicate, the results averaged and the error bars (± σ) reported in the relevant plots. The repetitions showed high robustness and reproducibility of the adopted experimental procedures.

2.4. Analysis

The concentration of 4-chlorophenol was measured through a YL9300 HPLC system equipped with a YL9330 Column Compartment and a YL9150 autosampler. The column was a RP C18 column (LiChroCART®, Merck, 12.5 cm × 0.4 cm; 5 μm packing). 4-chlorophenol was analyzed in isocratic mode using a 10:90% v/v acetonitrile:phosphoric acid solution (1×10^{-2} M) as mobile phase (flow rate of 1 mL min^{-1}, UV detection 220 nm). The retention time of 4-CP was 12 min. The CECs mixture was analyzed through the same instrument using as mobile phase acetonitrile and phosphoric acid solution (1×10^{-2} M) with the following gradient: 0 min, 80:20 v/v; 10 min, 65:35 v/v; 20 min, 35:65 v/v; 25 min, 80:20 v/v (flow rate of 1 mL/min, UV detection 200 nm). The retention times of the analyzed CECs were 5-Tolylbenzotriazole: 6.0 min; Carbamazepine: 12.1 min; Bisphenol A: 15.5 min; Ibuprofen: 22.1 min. The mineralization of 4-CP and the other investigated CECs could not be followed by monitoring the TOC concentration during the degradations due to the slight leaching of the HA coating. This was previously observed with similar materials [35].

TC, IC and TN were measured using a Shimadzu TOC-5000 analyzer (catalytic oxidation on Pt at 680 °C). The calibration was performed using standards of potassium phthalate, NaHCO$_3$/Na$_2$CO$_3$ and KNO$_3$.

The determination of Fe released in solution was evaluated by a spectrophotometric procedure. The total iron was determined by reducing the Fe(III) to Fe(II) with ascorbic acid (4×10^{-4} M) and complexing the Fe(II) with phenanthroline (4×10^{-3} M) in acidic conditions (buffer pH = 3: H$_3$PO$_4$ 1 mmol L^{-1}, NaH$_2$PO$_4$ 3 mmol L^{-1}). The Fe(II) was determined in the same way, without the reduction step, and Fe(III) was obtained as the difference between total iron and Fe(II) [46]. The calibration was performed using a commercial standard solution of Fe(III) (1000 mg^{Fe} L^{-1}, Sigma-Aldrich). The spectrophotometric analyses were performed using a Varian CARY 100 Scan double-beam UV–vis spectrophotometer, using quartz cuvettes with 10 mm path length and working at 510 nm.

3. Results and discussion

3.1. Materials characterization

The morphology of the synthesized MPs was investigated by SEM. Fig. S1 of the Supplementary Material (SM) shows the recorded micrographies. The adopted method of synthesis gave very heterogeneous samples composed of aggregates of primary particles with dimensions that ranged from tens of μm to sub-micrometer dimensions. Furthermore, no correlation between the particles texture and the amount of HA used during the synthesis was observed, as well as there was no clear difference in the morphology of the MPs synthesized in anoxic condition and in air. The HR-TEM analyses of analogous MPs were carried out by Magnacca et al. [47] and Carlos et al. [48]. They observed nanometric particles roughly spherical in shape (average particle size in the 10 nm range), with a crystalline core and an external layer of organic matter with less than 1 nm thickness. The TGA curves recorded under air on MPs/HA and bare magnetite are shown in Fig. S2 of SM. The first slight weight loss (30–150 °C) was related to the loss of physisorbed water, whereas - from the comparison between the pure magnetite and the hybrids TGA profiles - that in the 200–800 °C range was assigned to the loss of the chemically adsorbed HA coating due to

the combustion of the organic fraction. Weight losses calculated in the 200–800 °C range revealed a higher HA loading on the MPs when prepared in the presence of higher HA concentration (Table S1 and Fig. S2).

X-ray diffraction (XRD) patterns for MP/HA (Fig. S3) showed reflections at $2\theta = 30.1°$, $35.4°$, $43.0°$, $53.9°$, $57.2°$, and $62.6°$, in agreement with the reflections produced by the (2 2 0), (3 1 1), (4 0 0), (4 2 2), (5 1 1), and (4 4 0) planes of reference magnetite [49,50]. The Scherrer analysis of the peak related to the (3 1 1) plane gave a rough estimation of the crystalline domains in the 12–16 nm range in agreement with the HR-TEM micrographs of the primary particles previously reported [47,48].

The FTIR spectra of HA, Fe_3O_4 and Fe_3O_4/HA MPs are shown in Fig. S4. In the HA spectra the peak at ~3400 cm^{-1} was attributed to the stretching vibrations of –OH groups; 2920 cm^{-1} and 2850 cm^{-1} were assigned to CH_2, –CH_3 species; the ~1600 cm^{-1} and ~1400 cm^{-1}, were attributed to the stretching of –COOH groups. The peak with strong absorption at ~550 cm^{-1} shown on Fe_3O_4 MPs spectra was attributed to Fe-O bond. The intensity increase of the organic matter-related peaks was observed on Fe_3O_4/HA MPs spectrum confirming the HA coating on magnetite structure. These results were in agreement with the literature [48,51].

Additionally, Magnacca et al. reported on analogous materials that *i)* the point of zero charge – evaluated through the measuring of the zeta potentials (ζ) at different pH - changed from 7.2 on the bare Fe_3O_4 to 3.0 for the HA coated materials as a consequence of the presence at the surface of carboxylic and phenolic moieties; *ii)* the samples exhibited superparamagnetic characteristics, including zero coercivity and remanence [47].

X-ray photoelectron spectroscopy (XPS) analyses were performed on MPs prepared using different amounts of HA, both in anoxic and oxygenated conditions aiming at evaluating the effect of synthesis experimental conditions on the surface chemical composition and possibly correlating it to the observed reactivity in pollutants degradation. XPS has been largely used since long time to distinguish and to quantify Fe^{2+} and Fe^{3+} species [52,53]. These oxidation states can be indeed easily evaluated by Fe 2p region, considering chemical shift and multiplet splitting occurring for these species. Several examples of XPS application to iron oxide species have been reported, including nanoparticle and magnetic systems [53,54]. Fitting of the Fe 2p region requires the knowledge of the standard spectra of potential present iron oxide species, such as FeO, Fe_3O_4, Fe_2O_3 (namely α-Fe_2O_3 and γ-Fe_2O_3) and FeOOH (namely α-FeOOH and γ-FeOOH). In this regard, a very accurate work, which was used for interpreting our results, is reported in the literature [55]. In the survey spectra (data not shown), the major peaks were represented, as expected, by C 1 s, O 1 s and Fe 2p, with the presence of traces of S 2p, Cl 2p and N 1 s originating from $FeCl_3$, $FeSO_4$ and NH_4OH used in the synthesis. For a more detailed analysis, high-resolution XPS Fe 2p spectra were recorded. These spectra were fitted using multiplet peaks: an example is reported in Fig. 1, referred to Fe_3O_4/0.5HA prepared under anoxic environment. All investigated samples resulted to be very similar in terms of Fe 2p speciation being in all cases characterized by multiplet peaks which can be ascribed to Fe^{3+} of an oxidized form of iron, possibly γ-FeOOH on the basis of literature data [55], suggesting a higher degree of oxidation of surface MPs in comparison to bulk. As shown in Fig. 1, two peaks can be identified, denoted as pre-peak and surface peak, located at 708.7 eV and 713.6 eV, respectively. The low-intensity pre-peak on the low-binding-energy (BE) side of the envelope accounts for the formation of Fe ions with a lower than normal oxidation state by the production of defects (in which iron is in different coordination conditions – usually lower – than on the ordered crystallographic planes) in neighboring sites [55]. The high-BE surface peak referred to surface defective structures exhibiting different binding energies compared with that of the bulk structure because of surface termination, which frequently could result in a decreased symmetry [55]. Interestingly, while the

abundance of pre-peak was almost similar in all investigated samples, a remarkable variation of surface peak intensity was observed with varying particle synthesis experimental conditions, as reported in Fig. 1. It can be observed that, for samples prepared under nitrogen environment, the percentage area of surface peak increased when passing from bare MPs to ones prepared with HA 0.5 wt%, then decreasing to values slightly lower than that recorded on Fe_3O_4. These results well correlated with the observed particles activity of the studied heterogeneous catalysts (highest reactivity for Fe_3O_4/0.5HA, *vide infra*) suggesting an active role of these surface sites during the photo-activated degradation process on the investigated MPs (see section 3.2). In the case of materials prepared in air (data not shown), no significant difference was observed between Fe_3O_4 and Fe_3O_4/0.5HA, being in both cases the estimated abundance of surface peak similar to that of bare samples prepared in anoxic conditions. Finally, the presence of surface HA can be estimated from O 1 s high-resolution signal, as shown in Fig. 2, reporting the comparison among O 1 s spectra of Fe_3O_4 and some of the analyzed samples prepared in anoxic conditions. With the increase of humic acid percentage, an increase of two component peaks at about 532 eV and 534 eV can be observed, attributed to HA on the basis of the comparison with O 1 s spectrum of HA alone, thus suggesting that the actual surface amount of HA reflects the one used in the preparation of the particles.

3.2. Fenton- and photo-Fenton-like degradation of 4-chlorophenol

Preliminary experiments were performed in order to evaluate the efficiency of all MPs towards the degradation of 4-CP at pH 3 (the optimum pH in the homogeneous Fenton reaction). The possible 4-CP adsorption by the MPs was investigated by comparing the nominal concentration of pollutant and that recorded in solution at the end of the equilibration time (see section 2.3). Neither significant adsorption nor degradation were observed in the presence of MPs alone (less than5%). During degradation experiments, in the presence of MPs/HA under irradiation, the pH value was measured over time and comparing the initial pH with that measured at the end of the degradation no significant change over time was observed (ΔpH ≤ 0.1). Fig. 3 shows the results obtained for both, Fenton and photo-Fenton, revealing an increase on the 4-CP degradation for HA coated MPs comparing with bare Fe_3O_4, in agreement with the literature [56]. The photolysis of H_2O_2 in the adopted irradiation conditions and in the absence of MPs led to negligible 4-CP abatement (see Fig. 3b). The MPs prepared by adding 0.5 wt% of HA solution promoted 4-CP complete degradation after less than 5 min of irradiation or 30 min in the dark (note the different time axis between Fig. 3a and Fig. 3b), while the 4-CP degradation decreased in the presence of MP/HA prepared with higher or lower HA amounts.

In the dark, in all cases except for the bare Fe_3O_4, it was observed an exponential decay for 4-CP with the irradiation time, $C/C_0 = \exp(-k \times t)$, where C_0 and C are the substrate initial concentration and after the reaction time t, respectively and k is the pseudo first-order kinetic constant of the process. This gave an indication of a constant production of reactive species during the time interval. The 4-CP observed disappearance on Fe_3O_4 followed a different behavior with a sigmoidal profile easily fitted by the equation $C/C_0 = \exp(a + b \times t + c \times t^2)$, where a, b, and c are the fitting constants (see data shown in Table S2). In this case, it was observed that the process did not follow a first order kinetic, but the observed rate in the beginning of the reaction was lower. During the first minutes of reaction the system generated/cumulated active forms of iron (e.g. Fe(II) in solution and/or Fe^{2+} species at the surface) able to activate the degradation. This would explain the sigmoidal profile and the activation time observed and previously reported on bare magnetite [25]. Note that the sigmoidal fitting curves reported in Fig. 3 (and later) have no kinetic meaning and they were reported to help following the degradation profiles and to underline that in these cases the mechanism of
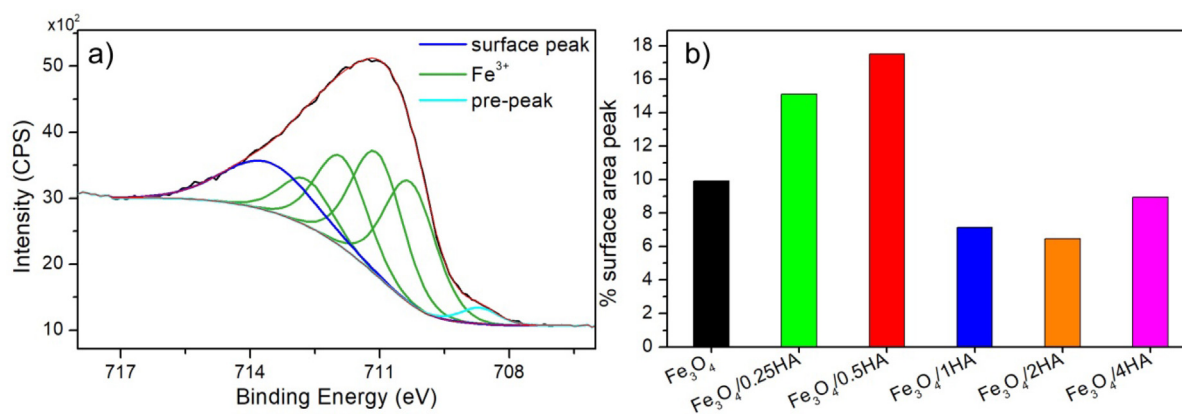
Fig. 1. High-resolution spectrum of Fe 2p region of $Fe_3O_4/0.5HA$ prepared under anoxic conditions (a). Spectrum is charging corrected. Percentage of the surface peak in all samples prepared in anoxic conditions (b).
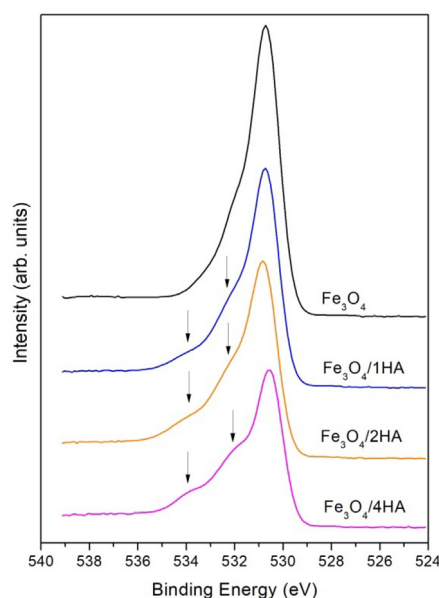

Fig. 2. High-resolution spectra of O 1 s region of selected MPs samples prepared under anoxic conditions. Arrows indicate component peaks increasing with the HA increase. Spectra are charging corrected.

transformation is more complex than a process simply described with a pseudo-first order kinetic process in which the concentration of reactive species reaches the steady state condition.

Under irradiation it was observed an increase of the 4-CP

degradation rate in all cases with a total disappearance of 4-CP before 20 min of irradiation. A pseudo first-order transformation was observed only with $Fe_3O_4/0.5HA$ and $Fe_3O_4/1HA$ which showed the fastest transformation rate. In all other cases a sigmoidal behavior was observed. Also, it was possible to suppose the presence of a process able to produce catalytic species that, once sufficiently accumulated in the system, were able to efficiently react with H_2O_2 promoting a fast substrate transformation.

The pH influence was investigated by adjusting the pH to 3, 4, 4.5 and 5. At the explored experimental pH range 4-CP exists as neutral specie being its pK_a = 9.4 [41]. Moreover, based on the data present in the literature for similar materials [35], reporting zero point charge of 2.3, we can assume that also in the present case the surface charge of MPs is negative in the explored pH range. Therefore, the working pH explored (from 3 to 5) had no impact on the 4-CP adsorption on MPs surface because the coulombic interaction between the neutral substrate and the negatively charged surface [35] did not change in this quite narrow pH range, as confirmed by the negligible difference between the nominal 4-CP concentration and the one measured in solution after the equilibration time. As a consequence, any eventual change in the reactivity at the different explored pH could not be related to changes in the adsorption of the substrate at the MPs surface.

Fig. 4 shows the disappearance of 4-CP under irradiation in the presence of the two best performing materials, namely $Fe_3O_4/0.5HA$ and $Fe_3O_4/1HA$, comparing with Fe_3O_4. For all pH the $Fe_3O_4/0.5HA$ showed the fastest degradation comparing with $Fe_3O_4/1HA$ and more clearly with Fe_3O_4. For all materials it was observed a decrease of the transformation rate increasing the pH. Analogous results were observed for the experiments performed in the dark, pointing out a slower abatement comparing with the irradiated system (Fig. S5).
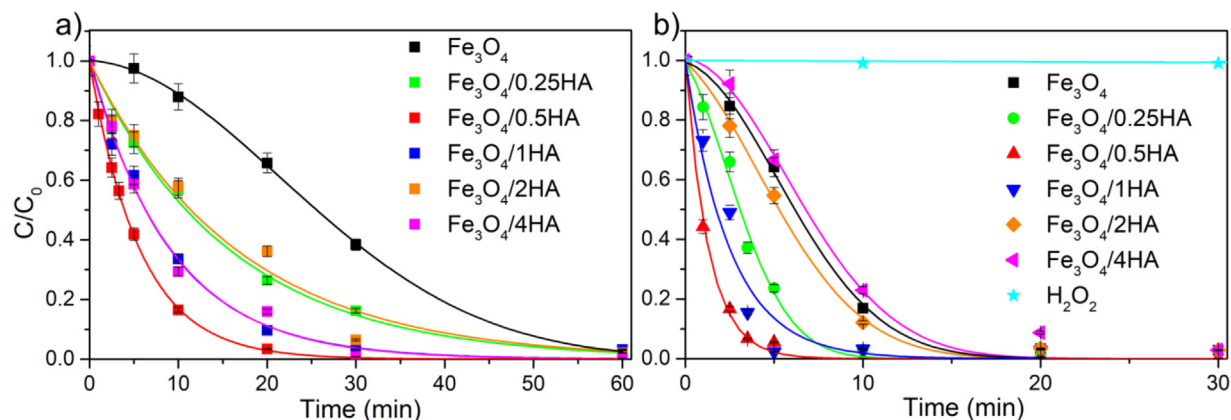

Fig. 3. Fenton-like (a) and photo-Fenton-like (b) degradation of 4-CP. Conditions: C_0 = 0.2 mmol L^{-1}, $[H_2O_2]$ = 1.0 mmol L^{-1}, [MPs] = 100 mg L^{-1}, pH 3.
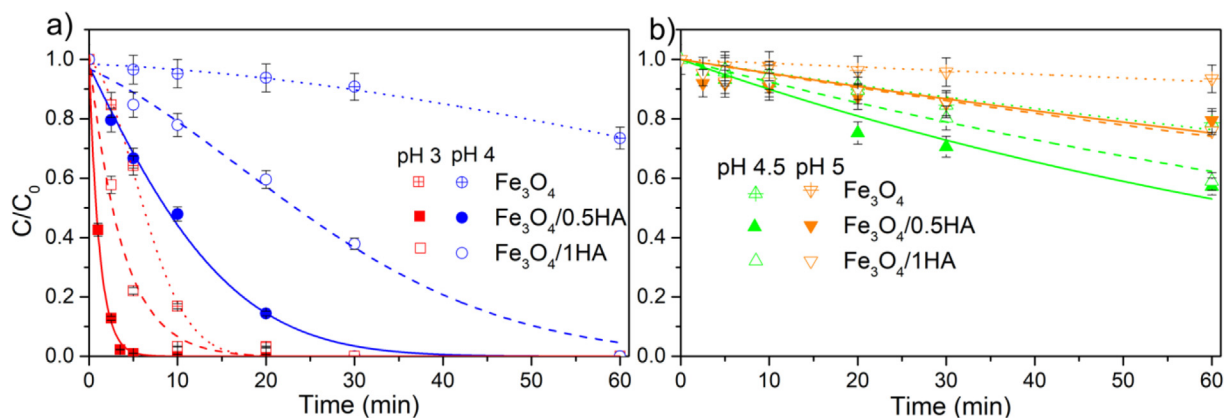
Fig. 4. Photo-Fenton-like degradation of 4-CP (0.2 mmol L^{-1}) with H_2O_2 (1.0 mmol L^{-1}) and 100 mg L^{-1} MPs at adjusted pH (3, 4, 4.5 and 5). Crossed open symbols: bare materials; solid symbols: $Fe_3O_4/0.5HA$; open symbols: $Fe_3O_4/1HA$.

An effective degradation of 4-CP was observed up to pH 4, at pH 4.5 the process was yet operative, although with slower kinetics, only under irradiation. At pH 4.5 in the dark the 4-CP degradation was blocked. As recently reported for the degradation of Ibuprofen [57], the impact of changing the operative pH from 3 to 4 is not negligible on the overall economic balance of a Fenton process. In particular, the shift of the pH from 3 to 4 can save costs related to the pH adjusting reagents of roughly 30%; note that the cost of the pH adjusting reagents accounts for an important fraction (roughly 40%) of the overall cost of the reagents used to carry out a thermal Fenton process [21].

The 4-CP main transformation products were identified as hydroquinone and benzoquinone by comparing the retention times of original standards. These hydroxylated products resulted from the electrophilic attack on the aromatic ring of 4-CP presumably by the generated hydroxyl radicals, as previously observed in thermal Fenton and Fenton-like processes [58,59]. The observed transformation products suggested a dominant role of the hydroxyl radicals as reactive species in the adopted experimental conditions. This was recently demonstrated with the same materials and in similar conditions through competitive experiments by using isopropanol as selective ·OH scavengers [60].

3.2.1. Iron release in solution

Several previous studies, dealing with the use of magnetite-based materials in Fenton-like and photo-Fenton-like processes, reported a strongly dependency of the efficiency on the dissolution of iron, revealing that the oxidation proceeds mostly *via* homogeneous Fenton [25]. The total amount of Fe released in solution at pH = 3 and its Fe (II)/Fe(III) speciation were determined spectrophotometrically. The effect of HA on the MPs iron leaching was evaluated by comparing the $Fe_3O_4/0.5HA$ and $Fe_3O_4/1HA$ behavior with the Fe_3O_4 in the presence and absence of H_2O_2 and upon irradiation or in the dark (Fig. 5). Since

the free-Fe(II) released in solution, for both, $Fe_3O_4/0.5HA$ (Fig. 5a) and $Fe_3O_4/1HA$ MPs (Fig. 5b) was $\sim 0.8 \times 10^{-2}$ mmol L^{-1} at time zero compared to $\sim 0.3 \times 10^{-2}$ mmol L^{-1} observed for Fe_3O_4 MPs (Fig. 5c), an intrinsic effect can be attributed to the HA. As expected, for all MPs the free-Fe(II) in solution decreased in the presence of H_2O_2 due to its oxidation to Fe(III) and consequent production of ·OH. The amount of iron released in solution was higher with $Fe_3O_4/0.5HA$ than in the presence of the bare Fe_3O_4 and $Fe_3O_4/1HA$ both in the dark and under irradiation. Moreover, an increase on iron leaching was observed for all MPs upon irradiation clearly indicating the photodissolution of the catalyst as previously reported [25]. The iron released in solution, at higher rate under irradiation, was mainly Fe(II) probably due to the lower product of solubility values (K_{ps}) of the Fe(III) hydroxides with respect to Fe(II) hydroxides. The highest dissolution observed with $Fe_3O_4/0.5HA$ is in agreement with the XPS analysis that showed a surface richer of surface defective structures, presumably more prone to be (photo)dissolved. The iron released in the best condition for the substrate degradation (i.e. under irradiation, pH 3, H_2O_2) was always below the limit for the discharge of water in surface bodies imposed by the common environmental legislations (e.g. for the Italian legislation the limit is 3.6×10^{-2} mM [61]). This means that in a real scenario at the end of the treatment the water might be discharged without any additional treatment for the abatement of the iron.

To evaluate the contribution of Fe(II)/Fe(III) ions released in solution on H_2O_2 activation, degradation experiments were performed by adding 4-CP and H_2O_2 to the supernatant.

Fig. 6 shows the 4-CP degradation upon irradiation for $Fe_3O_4/0.5HA$ and $Fe_3O_4/1HA$ supernatants solutions. 4-CP abatement was observed for both systems. This effect was attributed to homogeneous reactivity promoted by the dissolved iron. However, the 4-CP abatement was considerably lower if compared to the same experiments
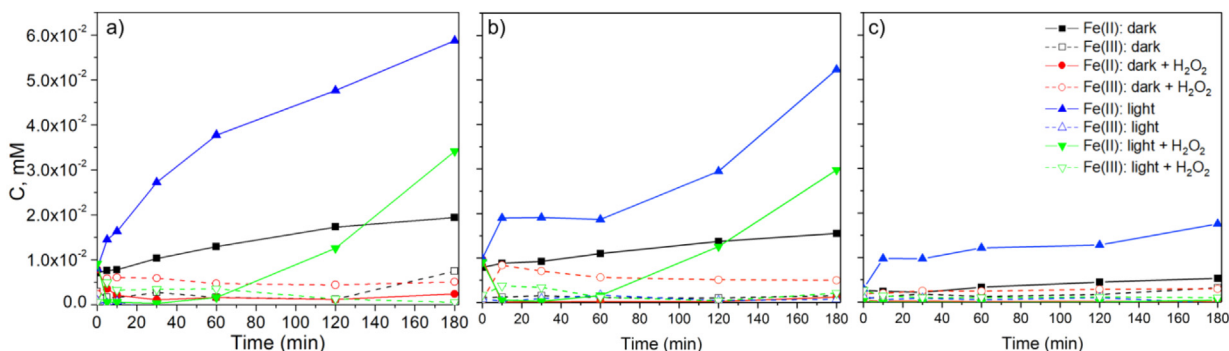

Fig. 5. Fe(II) and Fe(III) released in solution, in the dark and under irradiation, at pH 3 in the presence or absence of H_2O_2 (1 mmol L^{-1}) after removing the 100 mg L^{-1} of $Fe_3O_4/0.5HA$ (a); $Fe_3O_4/1HA$ (b) and Fe_3O_4 (c).
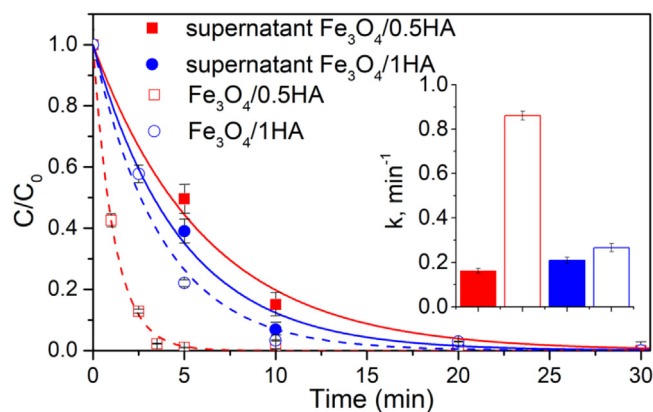
Fig. 6. Effect of iron ions released in solution on the 4-chlorophenol (0.2 mmol L^{-1}) abated in the presence of H_2O_2 (1.0 mmol L^{-1}) at pH 3 with Fe_3O_4/0.5HA and Fe_3O_4/1HA (100 mg L^{-1}) under irradiation. Inset: first-order kinetic constants of the process.

performed in the related heterogeneous conditions.

The results shown in Fig. 6 highlighted the active role of the Fe_3O_4/HA MPs either as iron reservoir that produced continuously active Fe(II) species at the surface or in solution (especially under irradiation) or as support of catalytic sites where efficient electron transfer between Fe(II) species and H_2O_2 occurred. The second hypothesis seems to be more robust. The comparison between the kinetics of dissolution (relatively slow, see the time axis of Fig. 5) and that of 4-CP degradation in the best experimental conditions (i.e. 4-CP half-time in the 0.5–1 min range, at pH 3 and under irradiation) suggested an operative role of the surface sites, and consequently a process that occurred mainly at the solid/liquid interface. Indeed, the significant difference between the degradation rates observed in the supernatant and in the related heterogeneous conditions cannot be rationalized simply on the basis of the role of iron reservoir for the MPs.

To better understand the impact of inert atmosphere during the materials synthesis, the MPs prepared with 0.5 wt% of HA in air atmosphere (ox-Fe_3O_4/0.5HA) were tested toward 4-CP. Fig. 7 shows a lower degradation rate for the ox-Fe_3O_4/0.5HA, both in dark and upon irradiation, comparing with the material prepared under inert atmosphere. Moreover, the kinetic profile observed when using ox-Fe_3O_4/0.5HA under irradiation features a sigmoidal shape, analogously to the 4-CP disappearance observed on Fe_3O_4 (Fig. 3). According to these results, the enhancement of the H_2O_2 activation from the materials prepared under nitrogen might be attributed to the higher bulk Fe(II)/Fe(III) ratio, as manifest by its non-reddish color.
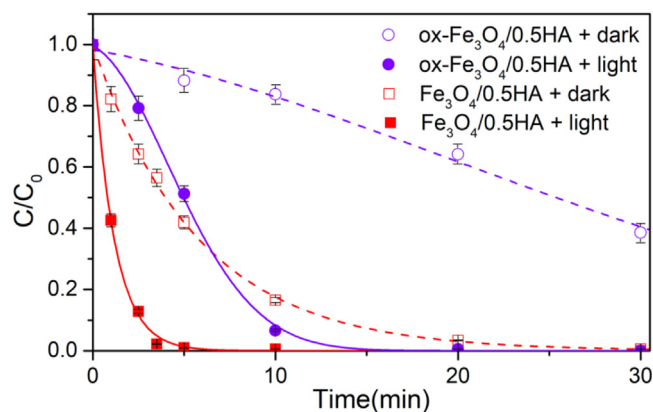

Fig. 7. Degradation of 4-CP (0.2 mmol L^{-1}) in the presence of ox-Fe_3O_4/0.5HA and Fe_3O_4/0.5HA (100 mg L^{-1}) at pH 3 and H_2O_2 (1.0 mmol L^{-1}), in the dark and under irradiation.

3.3. Photodegradation of CECs

The best performing material, namely Fe_3O_4/0.5HA, was tested toward 4 CECs commonly found in the environment, belonging to different categories and with distinctive chemical structure, representing a wide range of water pollutants, precisely: bisphenol A (BPA, a phenolic compound used in plastic industry), ibuprofen (IBU, an aromatic carboxylic acid used as anti-inflammatory drug), carbamazepine (CBZ, a tricyclic compound with a carboxamides functional group used as psychiatric drug) and 5-tolylbenzotriazole (5-TBA, a corrosion inhibitor with a benzotriazole ring). The molecular structure of the investigated CECs is reported in Fig. S6. The CECs abatement was tested separately in a single-compound experiment with the initial concentration of 0.2 mmol L^{-1}, excepting the CBZ (0.1 mmol L^{-1}) for solubility reasons. The Fenton-like and the photo-Fenton-like activity were evaluated in the dark and under irradiation, at pH 3 and 4, in the presence of 100 mg L^{-1} of Fe_3O_4/0.5HA and adding 1.0 mmol L^{-1} of H_2O_2 (Fig. 8). Based on the pK_a values of the investigated compounds, only 5-TBA was present as cation in all the investigated pH range, while the other compounds were in their neutral form. The effect of the pH on the CECs degradation was the same for all pollutants being the most efficient condition at pH 3. It was observed a degradation higher than 80% of BPA, CBZ and 5-TBA after 1 h under irradiation, while only 35% of IBP was removed. From the experimental results reported in Fig. 8, it is not possible to evidence any significant effect of neutrality/charge at pH 3; indeed BPA (neutral) and 5-TBA (cation) featured similar degradation profile.

At pH 4 a significant degradation was observed only for BPA, under irradiation, while CBZ, IBP and 5-TBA were only partially removed. The extension up to pH 4 of the reactivity of Fe_3O_4/0.5HA was previously reported for 4-CP (see above): the presence of phenolic moieties seemed to promote an effective removal of the substrate. The highest reactivity toward BPA can be explained considering that BPA is, among the CECs investigated, the compound with the highest second order kinetic constant with ·OH (1.55×10^{10} M^{-1} s^{-1} [62]), while IBP is that with the lowest one (6.5×10^9 M^{-1} s^{-1} [62]). This suggests a dominant role of the ·OH as reactive species in the investigated process as usually reported for the (photo)Fenton processes carried out in acidic conditions [56] and in agreement with the main transformation products identified during the 4-CP degradation.

3.3.1. Effect of water matrix

In order to evaluate a more representative system of a real scenario, the efficiency of Fe_3O_4/0.5HA was also tested in real wastewater spiked with a CECs mixture at lower concentration (C_0 = 20 μM). The degradation profiles are shown in Fig. 9 together with the observed kinetic constants. Despite the high concentration of organic and inorganic constituents in the wastewater samples, the obtained results showed no decrease on CECs removal efficiency comparing with results obtained in Milli-Q® water (Fig. 9a). In fact, a slight increase on degradation kinetic constants was observed, being the material able to completely abate the pollutants within 1 h of irradiation. Considering the presence of organic (mainly the dissolved organic matter) and inorganic constituents (mainly inorganic carbon (HCO_3^-/CO_3^{2-}), but also other reactive anions, e.g. Cl^- and NO_3^-) in wastewater sample that can compete for the reactive species, these results were rather surprising and support the possible application of this process for the abatement of recalcitrant pollutants in real wastewaters.

4. Conclusions

Humic acid coated Fe_3O_4 magnetic particles prepared *via* co-precipitation method under inert atmosphere were highly efficient to abate 4-CP in Fenton-like and photo-Fenton-like conditions and showed an enhanced activity when compared with the bare magnetite.

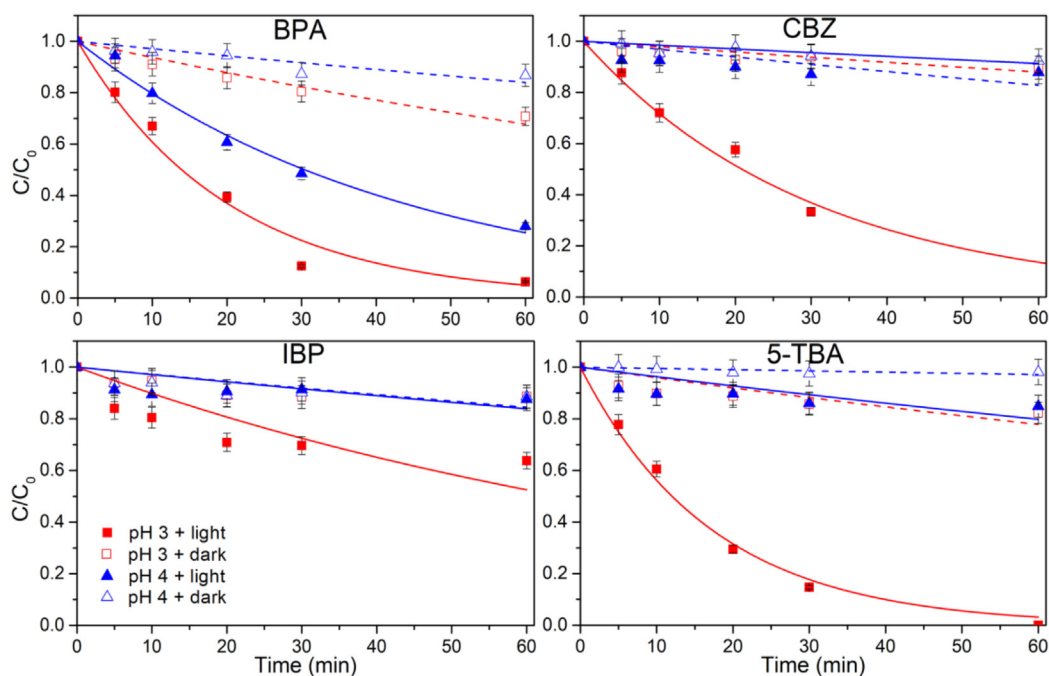Thanks to XPS experiments it was possible to evidence a

Fig. 8. Fenton-like and photo-Fenton-like degradation of each CEC separately ($C_O^{BPA,IBP,5-TBA}$ = 0.2 mmol L^{-1}; C_O^{CBZ} = 0.1 mmol L^{-1}) at pH 3 and 4, in the presence of H$_2$O$_2$ (1.0 mmol L^{-1}) and Fe$_3$O$_4$/0.5HA (100 mg L^{-1}).

structure–reactivity relationship for MPs, suggesting an active role of the more defective iron species at the surface to promote faster degradations due to not only a faster photodissolution of the iron phase, but also to a higher reactivity at the catalyst surface. Although the iron ions leached into solution had a remarkable influence in the oxidation process, a relevant role can therefore be imputed to processes at the solid/liquid interface (heterogeneous reactivity).

The experiments carried out with a CECs mixture showed that Fe$_3$O$_4$/0.5HA is a promising catalyst for heterogeneous (photo)-Fenton process at pH lower than 4, particularly active towards compounds with phenolic moieties also in wastewater.

This result, together with the good reusability of Fe$_3$O$_4$/0.5HA previously reported [60], opens the possibility of developing advanced tertiary treatments for the removal of CECs from urban wastewater by employing cheap and environmentally friendly materials and reagents (e.g. H$_2$O$_2$) and activating the process through the widely diffused and inexpensive solar irradiation.

Declaration of Competing Interest

The authors declare that they have no known competing financial interests or personal relationships that could have appeared to influence the work reported in this paper.

Acknowledgements

Appendix A. Supplementary data

Supplementary data to this article can be found online at https://doi.org/10.1016/j.cej.2020.124619.

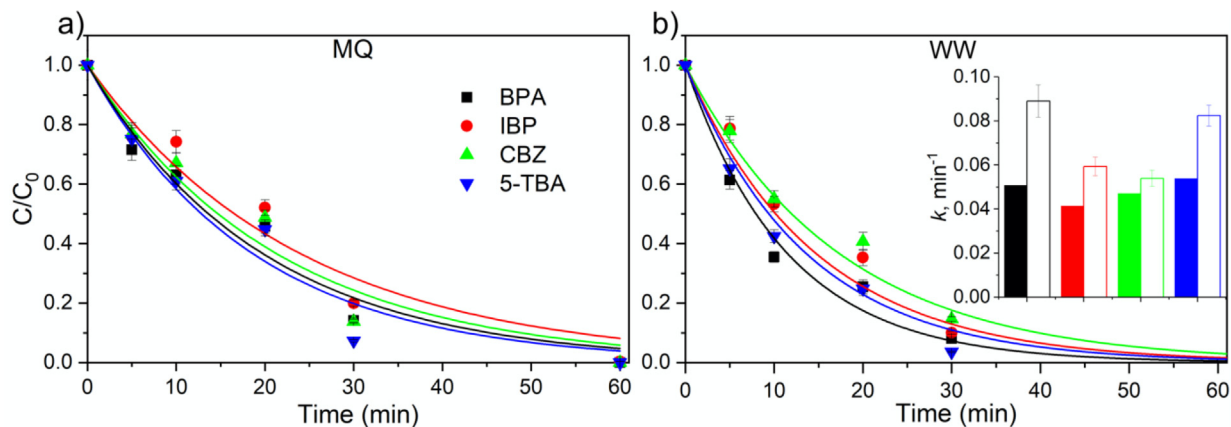**Fig. 9.** Photo-Fenton-like degradation of CEC mixture (20 μM) in a) Milli-Q® water (MQ) and b) real wastewater (WW) sample at pH 3, in the presence of H$_2$O$_2$ (1.0 mmol L^{-1}) and Fe$_3$O$_4$/0.5HA (100 mg L^{-1}). Inset: first-order kinetic constants of the process carried out in Milli-Q® water (solid bars) and wastewater (open bars).

References

[1] A. Gogoi, P. Mazumder, V. Kumar, G.G.T. Chaminda, A. Kyoungjin, M. Kumar, Occurrence and fate of emerging contaminants in water environment: a review, Groundw. Sustain. Dev. 6 (2018) 169–180.

[2] M. Taheran, M. Naghdi, S.K. Brar, M. Verma, R.Y. Surampalli, Emerging contaminants: Here today, there tomorrow!, Environ. Nanotechnol. Monit. Manag. 10 (2018) 122–126.

[3] S.D. Richardson, T.A. Ternes, Water analysis: emerging contaminants and current issues, Anal. Chem. 90 (2018) 398–428.

[4] J. Wilkinson, P.S. Hooda, J. Barker, S. Barton, J. Swinden, Occurrence, fate and transformation of emerging contaminants in water: an overarching review of the field, Environ. Pollut. 231 (2017) 954–970.

[5] Y. Deng, R. Zhao, Advanced Oxidation Processes (AOPs) in Wastewater Treatment, Curr. Pollut. Reports. 1 (2015) 167–176.

[6] M. Salimi, A. Esrafili, M. Gholami, A. Jonidi Jafari, R. Rezaei Kalantary, M. Farzadkia, M. Kermani, H.R. Sobhi, Contaminants of emerging concern: a review of new approach in AOP technologies, Environ. Monit. Assess. 189 (2017) 414–436.

[7] H. Lu, J. Wang, F. Li, X. Huang, B. Tian, H. Hao, Highly efficient and reusable montmorillonite/Fe$_3$O$_4$/humic acid nanocomposites for simultaneous removal of Cr (VI) and aniline, Nanomaterials 8 (2018) 537–552.

[8] Z. Chen, H. Yi, M. Cheng, M. Zhang, G. Zeng, X. Liu, L. Chen, L. Li, L. Qin, B. Li, C. Lai, D. Huang, Fabrication of CuS/BiVO$_4$ (0 4 0) binary heterojunction photocatalysts with enhanced photocatalytic activity for Ciprofloxacin degradation and mechanism insight, Chem. Eng. J. 358 (2018) 891–902.

[9] S. Wacławek, H.V. Lutze, K. Grübel, V.V.T. Padil, M. Černík, D.D. Dionysiou, Chemistry of persulfates in water and wastewater treatment: a review, Chem. Eng. J. 330 (2017) 44–62.

[10] M.C. Pereira, L.C.A. Oliveira, Iron oxide catalysts: Fenton and Fenton-like reactions - a review, Clay Miner. 47 (2012) 285–302.

[11] S. Enami, Y. Sakamoto, A.J. Colussi, Fenton chemistry at aqueous interfaces, Proc. Natl. Acad. Sci. 111 (2014) 623–628.

[12] W. Huang, M. Luo, C. Wei, Y. Wang, K. Hanna, G. Mailhot, Enhanced heterogeneous photo-Fenton process modified by magnetite and EDDS: BPA degradation, Environ. Sci. Pollut. Res. 24 (2017) 10421–10429.

[13] C. Minero, M. Lucchiari, V. Maurino, D. Vione, A quantitative assessment of the production of OH and additional oxidants in the dark Fenton reaction: Fenton degradation of aromatic amines, RSC Adv. 3 (2013) 26443–26450.

[14] H. Bataineh, O. Pestovsky, A. Bakac, pH-Induced mechanistic changeover from hydroxyl radicals to iron(IV) in the Fenton reaction, Chem. Sci. 3 (2012) 1594–1599.

[15] S.H. Bossmann, E. Oliveros, S. Göb, S. Siegwart, E.P. Dahlen, L. Payawan, M. Straub, M. Wörner, A.M. Braun, New evidence against hydroxyl radicals as reactive intermediates in the thermal and photochemically enhanced Fenton reactions, J. Phys. Chem. A. 102 (2002) 5542–5550.

[16] W. Huang, M. Brigante, F. Wu, C. Mousty, K. Hanna, G. Mailhot, Assessment of the Fe(III)-EDDS complex in Fenton-like processes: from the radical formation to the degradation of bisphenol A, Environ. Sci. Technol. 47 (2013) 1952–1959.

[17] Y. Wu, M. Passananti, M. Brigante, W. Dong, G. Mailhot, Fe(III)–EDDS complex in Fenton and photo-Fenton processes: from the radical formation to the degradation of a target compound, Environ. Sci. Pollut. Res. 12154–12162 (2014).

[18] A.D. Bokare, W. Choi, Review of iron-free Fenton-like systems for activating H$_2$O$_2$ in advanced oxidation processes, J. Hazard. Mater. 275 (2014) 121–135.

[19] F. Fu, D.D. Dionysiou, H. Liu, The use of zero-valent iron for groundwater remediation and wastewater treatment: a review, J. Hazard. Mater. 267 (2014) 194–205.

[20] P. Avetta, A. Pensato, M. Minella, M. Malandrino, V. Maurino, C. Minero, K. Hanna, D. Vione, Activation of persulfate by irradiated magnetite: Implications for the degradation of phenol under heterogeneous photo-fenton-like conditions, Environ. Sci. Technol. 49 (2015) 1043–1050.

[21] M. Minella, N. De Bellis, A. Gallo, M. Giagnorio, C. Minero, R. Bertinetti, R. Sethi, A. Tiraferri, D. Vione, Coupling of nanofiltration and thermal Fenton reaction for the abatement of carbamazepine in wastewater, ACS Omega 3 (2018) 9407–9418.

[22] C. Walling, Fenton's reagent revisited, Acc. Chem. Res. 8 (1975) 125–131.

[23] G. Ruppert, R. Bauer, G. Heisler, The photo-Fenton reaction – an effective photochemical wastewater treatment process, J. Photochem. Photobiol. A Chem. 73 (1993) 75–78.

[24] A. Mirzaei, Z. Chen, F. Haghighat, L. Yerushalmi, Removal of pharmaceuticals from water by homo/heterogonous Fenton-type processes – a review, Chemosphere 174 (2017) 665–688.

[25] M. Minella, G. Marchetti, E. De Laurentiis, M. Malandrino, V. Maurino, C. Minero, D. Vione, K. Hanna, Photo-Fenton oxidation of phenol with magnetite as iron source, Appl. Catal. B Environ. 154–155 (2014) 102–109.

[26] L. Demarchis, M. Minella, R. Nisticò, V. Maurino, C. Minero, D. Vione, Photo-Fenton reaction in the presence of morphologically controlled hematite as iron source, J. Photochem. Photobiol. A Chem. 307–308 (2015) 99–107.

[27] M. Munoz, Z.M. de Pedro, J.A. Casas, J.J. Rodriguez, Preparation of magnetite-based catalysts and their application in heterogeneous Fenton oxidation – a review, Appl. Catal. B Environ. 176–177 (2015) 249–265.

[28] D. Palma, A.B. Prevot, M. Brigante, D. Fabbri, G. Magnacca, C. Richard, G. Mailhot, R. Nisticò, New insights on the photodegradation of caffeine in the presence of biobased substances-magnetic iron oxide hybrid nanomaterials, Materials 11 (2018) 1–17.

[29] R.C.C. Costa, M.F.F. Lelis, L.C.A. Oliveira, J.D. Fabris, J.D. Ardisson, R.R.V.A. Rios, C.N. Silva, R.M. Lago, Novel active heterogeneous Fenton system based on Fe$_{3-x}$M$_x$O$_4$ (Fe, Co, Mn, Ni): The role of M^{2+} species on the reactivity towards H$_2$O$_2$ reactions, J. Hazard. Mater. 129 (2006) 171–178.

[30] W. Wu, Q. He, C. Jiang, Magnetic iron oxide nanoparticles: Synthesis and surface functionalization strategies, Nanoscale Res. Lett. 3 (2008) 397–415.

[31] F. Franzoso, R. Nisticò, F. Cesano, I. Corazzari, F. Turci, D. Scarano, A. Bianco Prevot, G. Magnacca, L. Carlos, D.O. Mártire, Biowaste-derived substances as a tool for obtaining magnet-sensitive materials for environmental applications in wastewater treatments, Chem. Eng. J. 310 (2017) 307–316.

[32] P. Singhal, S.K. Jha, S.P. Pandey, S. Neogy, Rapid extraction of uranium from sea water using Fe$_3$O$_4$ and humic acid coated Fe$_3$O$_4$ nanoparticles, J. Hazard. Mater. 335 (2017) 152–161.

[33] S. Koesnarpadi, S.J. Santosa, D. Siswanta, B. Rusdiarso, Humic acid coated Fe$_3$O$_4$ nanoparticle for phenol sorption, Indones. J. Chem. 17 (2017) 274–283.

[34] J.D. Hu, Y. Zevi, X.M. Kou, J. Xiao, X.J. Wang, Y. Jin, Effect of dissolved organic matter on the stability of magnetite nanoparticles under different pH and ionic strength conditions, Sci. Total Environ. 408 (2010) 3477–3489.

[35] J. Liu, Z. Zhao, G. Jiang, Coating Fe$_3$O$_4$ magnetic nanoparticles with humic acid for high efficient removal of heavy metals in water, Environ. Sci. Technol. 42 (2008) 6949–6954.

[36] L. Peng, P. Qin, M. Lei, Q. Zeng, H. Song, J. Yang, J. Shao, B. Liao, J. Gu, Modifying Fe$_3$O$_4$ nanoparticles with humic acid for removal of Rhodamine B in water, J. Hazard. Mater. 209–210 (2012) 193–198.

[37] L. Carlos, D.O. Mártire, M.C. Gonzalez, J. Gomis, A. Bernabeu, A.M. Amat, A. Arques, Photochemical fate of a mixture of emerging pollutants in the presence of humic substances, Water Res. 46 (2012) 4732–4740.

[38] S. Koesnarpadi, S.J. Santosa, D. Siswanta, B. Rusdiarso, Synthesis and characterizatation of magnetite nanoparticle coated humic acid (Fe$_3$O$_4$/HA), Procedia Environ. Sci. 30 (2015) 103–108.

[39] F. Aparicio, J.P. Escalada, E. De Gerónimo, V.C. Aparicio, F.S.G. Einschlag, G. Magnacca, L. Carlos, D.O. Mártire, Carbamazepine degradation mediated by light in the presence of humic substances-coated magnetite nanoparticles, Nanomaterials 9 (2019) 1–12.

[40] M. Bodrato, D. Vione, APEX (Aqueous Photochemistry of Environmentally occurring Xenobiotics): a free software tool to predict the kinetics of photochemical processes in surface waters, Environ. Sci. Process. Impacts. 16 (2014) 732–740.

[41] International Union of Pure and Applied Chemistry. Commission on Equilibrium Data, E.P. Serjeant, B. Dempsey, International Union of Pure and Applied Chemistry. Commission on Electrochemical Data., Ionisation constants of organic acids in aqueous solution, Pergamon Press, 1979.

[42] C.D. Herzfeldt, R. Kümmel, Dissociation constants, solubilities and dissolution rates of some selected nonsteroidal antiinflammatories, Drug Dev. Ind. Pharm. 9 (1983) 767–793.

[43] G. Zeng, C. Zhang, G. Huang, J. Yu, Q. Wang, J. Li, B. Xi, H. Liu, Adsorption behavior of bisphenol A on sediments in Xiangjiang River, Central-south China, Chemosphere 65 (2006) 1490–1499.

[44] M.D. Alotaibi, B.M. Patterson, A.J. McKinley, A.Y. Reeder, A.J. Furness, Benzotriazole and 5-methylbenzotriazole in recycled water, surface water and dishwashing detergents from Perth, Western Australia: analytical method development and application, Environ. Sci. Process. Impacts. 17 (2015) 448–457.

[45] O.A.H. Jones, N. Voulvoulis, J.N. Lester, Aquatic environmental assessment of the top 25 English prescription pharmaceuticals, Water Res. 36 (2002) 5013–5022.

[46] A.E. Harvey, J.A. Smart, E.S. Amis, Simultaneous spectrophotometric determination of iron(ll) and total iron with 1,10-phenanthroline, Anal. Chem. 27 (1955) 26–29.

[47] G. Magnacca, A. Allera, E. Montoneri, L. Celi, D.E. Benito, L.G. Gagliardi, M.C. Gonzalez, D.O. Mártire, L. Carlos, Novel magnetite nanoparticles coated with waste-sourced biobased substances as sustainable and renewable adsorbing materials, ACS Sustain. Chem. Eng. 2 (2014) 1518–1524.

[48] L. Carlos, M. Cipollone, D.B. Soria, M. Sergio Moreno, P.R. Ogilby, F.S. García Einschlag, D.O. Mártire, The effect of humic acid binding to magnetite nanoparticles on the photogeneration of reactive oxygen species, Sep. Purif. Technol. 91 (2012) 23–29.

[49] JCPDS Card No. 75-033, n.d.

[50] U. Panne, V.-D. Hodoroaba, A. Paul, G. Ababei, R.J. Schneider, M. Neamtu, C. Nadejde, Green Fenton-like magnetic nanocatalysts: Synthesis, characterization and catalytic application, Appl. Catal. B Environ. 176–177 (2015) 667–677.

[51] Y. Fu, Hong-bo; Quan, Xie; Chen, Shuo; Zhao, Hui-min; Zhao, Interactions of HA and hematite FTIR study, J. Environ. Sci. 17 (2005) 43–47.

[52] N.S. McIntyre, D.G. Zetaruk, X-ray photoelectron spectroscopic studies of iron oxides - Analytical Chemistry, Anal. Chem. 49 (1977) 1521–1529.

[53] R. Di Corato, A. Aloisi, S. Rella, J.M. Greneche, G. Pugliese, T. Pellegrino, C. Malitesta, R. Rinaldi, Maghemite nanoparticles with enhanced magnetic properties: one-Pot preparation and ultrastable dextran shell, ACS Appl. Mater. Interfaces 10 (2018) 20271–20280.

[54] T.C. Lin, G. Seshadri, J.A. Kelber, A consistent method for quantitative XPS peak analysis of thin oxide films on clean polycrystalline iron surfaces, Appl. Surf. Sci. 119 (1997) 83–92.

[55] A.P. Grosvenor, B.A. Kobe, M.C. Biesinger, N.S. McIntyre, Investigation of multiplet splitting of Fe 2p XPS spectra and bonding in iron compounds, Surf. Interface Anal. 36 (2004) 1564–1574.

[56] H. Niu, D. Zhang, S. Zhang, X. Zhang, Z. Meng, Y. Cai, Humic acid coated Fe$_3$O$_4$ magnetic nanoparticles as highly efficient Fenton-like catalyst for complete mineralization of sulfathiazole, J. Hazard. Mater. 190 (2011) 559–565.

[57] S. Bertinetti, M. Minella, K. Hanna, C. Minero, D. Vione, Degradation of ibuprofen with a Fenton-like process triggered by zero-valent iron (ZVI-Fenton), Environ. Res. 179 (2019) 108750.

[58] S. He, Y. Chen, H. Wang, W. Yang, Y. Gao, Y. Zhao, Degradation of 4-Chlorophenol

by means of Fenton oxidation processes: mechanism and kinetics, Water. Air. Soil Pollut. 228 (2017) 284–293.

[59] F. Duan, Y. Yang, Y. Li, H. Cao, Y. Wang, Y. Zhang, Heterogeneous Fenton-like degradation of 4-chlorophenol using iron/ordered mesoporous carbon catalyst, J. Environ. Sci. 26 (2014) 1171–1179.

[60] N.P.F. Gonçalves, M. Minella, G. Mailhot, M. Brigante, A. Bianco Prevot, Photo-activation of persulfate and hydrogen peroxide by humic acid coated magnetic particles for Bisphenol A degradation, Catal. Today. in press, 2019. Doi: 10.1016/j.cattod.2019.12.028.

[61] D. Lgs 152/06, https://www.gazzettaufficiale.it/atto/serie_generale/caricaDettaglioAtto/originario?atto.dataPubblicazione Gazzetta = 2006-04-14& atto.codiceRedazionale = 006G0171.

[62] S. Mandal, Reaction rate constants of hydroxyl radicals with micropollutants and their significance in advanced oxidation processes, J. Adv. Oxid. Technol. 21 (2018) 178–195.